

# Inlet Swirl and Dump Gap Effect on Static Pressure Recovery in Dump Diffuser-Combustor using Two Equation Turbulence Model



Ajay Kumar Sahu, Prakash Ghose

**Abstract:** Cold flow through an axi-symmetric dump diffuser, provided with a swirl effect at inlet is studied by using various two equation  $k-\epsilon$  turbulent models such as; standard  $k-\epsilon$ , RNG  $k-\epsilon$  and Realizable  $k-\epsilon$  model. There is a liner with a liner dome head of hemispherical in shape is used as a bluff body. From the comparison in between the three  $k-\epsilon$  turbulent models, it has been observed that the overall prediction of flow variables with Realizable  $k-\epsilon$  model are much better than others. The effects of dump gap and inlet swirl on velocity distribution and pressure variation on liner and casing walls have been investigated. The static pressure recovery within the diffuser is evaluated from area weighted average pressure at inlet and exit plane. It is noticed that an optimum inlet swirl results in the most effective pressure recovery due to the minimum irrecoverable energy dissipation in the vortices formed in the domain. The optimum swirl number is found to be 0.38 and it occurs when DG (non-dimensional dump gap) is kept as 1.0. The variation in dump gap changes the flow pattern and the possible pressure recovery. As the dump gap is increased, the static pressure is recovered more effectively with moderate swirl level in the inlet flow.

**Keywords :** Dump diffuser-combustor, swirl, dump gap, static pressure recovery.

## I. INTRODUCTION

The dump diffuser-combustor normally consists of a sudden expansion diffuser and a liner. The liner with a dome head is placed co-axially within the combustor casing. The purpose of the diffuser is to reduce the air velocity through sudden expansion opening. The air within the sudden expansion opening and the casing-liner annulus is fed in to the liner through the primary, secondary, and tertiary holes present on the liner wall. The main purpose for velocity reduction through dump diffuser is to avoid the flame blowout. The primary air helps to oxidize the fuel and secondary and dilution air complete the combustion and maintain a moderate temperature of flue gas. Dump diffuser-combustor is normally preferred in gas turbine engine because it makes the engine lighter by avoiding the use of heavy compressor. However investigation of velocity field and pressure distributions in the annulus are required in order to optimize the feed flow through the holes on the liner wall.

Revised Manuscript Received on March 30, 2020.

\* Correspondence Author

Ajay Kumar Sahu\*, School of Mechanical Engineering, KIIT University, Bhubaneswar, India. Email: sahu.ajay93@gmail.com

Dr. Prakash Ghose\*, School of Mechanical Engineering, KIIT University, Bhubaneswar, India. Email: pghosefme@kiit.ac.in

© The Authors. Published by Blue Eyes Intelligence Engineering and Sciences Publication (BEIESP). This is an [open access](#) article under the CC BY-NC-ND license (<http://creativecommons.org/licenses/by-nc-nd/4.0/>)

In a dump diffuser, boundary layer separation takes place at the dump plane, forming a recirculating vortex at the corner. Energy dissipation within the vortex results in an additional stall loss, thereby increasing the total aerodynamic loss across the combustor. Two factors can influence the overall pressure loss in the diffuser. Firstly, swirl in the flow approaching the diffuser causes quick flow reattachment to the outer wall and reduces the size of the recirculating vortex and the associated loss. Normally a light centrifugal compressor is coupled with turbine to feed the air into the combustor. Therefore the air enters in to the diffuser with a swirling motion. But too much swirl is undesirable because it causes a bad temperature pattern factor at combustor outlet, which affects the turbine life [1]. Sometime a set of guide vanes are used to prevent the swirl made by compressor, but still air enters to the diffuser with a certain degree of swirl. Secondly, a smaller dump gap (axial distance between the dump plane and the liner dome) produces flow curvature towards the outer wall, thereby affecting the vortex size. However, for the present day low NO<sub>x</sub> gas turbine combustors, the lean combustion requirement increases the size of the fuel injection module [2] necessitating a higher the dump gap. Therefore, an optimized flow condition in the gas turbine diffuser requires a suitable swirl level at its inlet and a proper dump gap.

Many researchers worked to investigate the flow field within the combustor both under isothermal [3], [4], [5] [6] and reactive [7], [8], [9], [10] flow conditions. These include experimental and numerical approaches to study flow mixing, combustion behavior, exit pattern factor, emission etc. Contrary to these, the flow behavior analysis in the diffuser and casing-liner annulus is rarely investigated, that has been observed from open literature. Fishenden and Stevens [11] reported the benefit of blockage effect by liner dome by maintaining a lower dump gap. But has been observed that too much reduction in the dump gap, increases the flow energy loss within the casing-liner annulus. Karki et al. [12] compare the prediction potential between a three dimensional and a simplified axi-symmetric computational model. It has been observed that both the models predict the static pressure recovery with a similar accuracy. Hestermann et al. [13] performed both experimental work and numerical simulation in a model combustor diffuser geometry having a pre-diffuser and a dump diffuser. Emphasis was given to study the flow in the pre-diffuser and investigating the maximum opening angle without flow separation. It was found that the location of the liner and the level of turbulence at the pre-diffuser inlet have dominating effects in deciding the angle. Walker et al. [2]

worked on designing the OGV(outer guide vane) in order to enhance the performance parameters like pressure recovery. By optimizing the OGV angle and pre-diffuser opening, the swirl level can be controlled, by which the reattachment length on the casing wall can be reduced. Walker et al. [14] also worked on the effect of dump gap to investigate the flow characteristics within the diffuser and pre-diffuser. Rahim et al. [15] performed experiment and investigated the impact of swirl on casing wall re-attachment length through the measurement of pressure distribution at liner and casing wall along axial direction. They also observed that a strong central recirculation zone (CTRZ) is appeared ahead of the dome head at a higher degree of swirl. Dome profile impact on pressure recovery also has been investigated by Rahim et al. [16]. It has been concluded that dome head with hemispherical profile a highest static pressure recovery has been obtained in presence of swirl.

Standard  $k-\varepsilon$  turbulent model has been used by various people for computational modeling of dump diffuser [12], [13], [17]. Advanced models like Reynolds stress model (under the scope of RANS) or large eddy simulation (LES) have been proposed in various literature [18], [19], [20], [21] for modeling flow in a combustor. However, these advanced models significantly increase either the computational cost or fails to give consistent advantages in the prediction over the  $k-\varepsilon$  models [22] [23].

Different variant of  $k-\varepsilon$  models are proposed to anticipate the performance of swirling turbulent flow in different physical situations. Escue and Cui [24] computed turbulent swirling flow in pipes at different swirl numbers and compared their predictions against experiments. It has been reported that RNG  $k-\varepsilon$  model [25] predicts well and good at low levels of swirl, on the other hand at higher degree of swirl, Reynolds Stress Model found to be more suitable. Zhu and Shih [26] predicted the flow of a confined jet in a cylindrical duct and observed that both RNG  $k-\varepsilon$  and standard  $k-\varepsilon$  model predicts similar results, while a realizable Reynolds stress algebraic equation model perform significantly better in resolving the essential flow features captured in the experiments. On the other hand, Karagoz and Kaya [27] validated the RNG  $k-\varepsilon$  model as the proper model for a strong swirling turbulent flow. Yajun et al. [28] made a comparative study between five different turbulence models by incorporating them in a simulation for a gas turbine combustor and suggested for realizable  $k-\varepsilon$  model. From the review of literature it has been observed that with a small change in either geometry or flow conditions a particular turbulent model fails to predict. Therefore it is difficult to suggest a turbulent model for a particular geometric and flow conditions.

In this study flow has been simulated across a dump diffuser opening and within the casing-liner annulus in an axi-symmetric model combustor. Three two-equation turbulent models, viz. standard  $k-\varepsilon$ , RNG  $k-\varepsilon$  and realizable  $k-\varepsilon$  model, are used and the result obtained are compared with experimental results. From the comparison the most suitable turbulent model has been chosen and used throughout the work to study the dump gap effect on flow pattern and pressure recovery.

## II. MODEL DESCRIPTION

By following the work of Rahim et. al. [16], an axi-symmetric 2D geometry is prepared. The schematic of

this axi-symmetric dump diffuser-combustor is shown in fig.1. The dimensional detail of the geometry is given in Table 1.

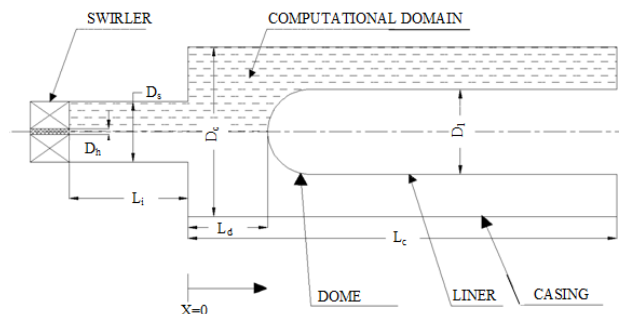


**Fig.1 Physical model and computational domain**

**Table-I: Dump diffuser-combustor dimensions**

Dimensions	Notation	Value (m)
Inlet pipe length	$L_i$	0.1
Casing length	$L_c$	0.4572
Swirler outer diameter	$D_s$	0.054
Hub diameter	$D_h$	0.005
Casing diameter	$D_c$	0.1524
Liner diameter	$D_l$	0.0762
Dump gap distance	$L_d$	0.0672, 0.1524, 0.2268
Non dimensional length	$L$	$X/D_c$
Dump gap	DG	$L_d/D_l$
Swirler vane angle		$0^\circ, 15^\circ, 30^\circ, 45^\circ$
Swirl number	SN	0, 0.178, 0.38, 0.67

### A. Governing Equations

The flow field within the computational domain is obtained by solving the time averaged continuity equations and RANS equation in the cylindrical coordinate system under steady state condition. The governing equations are expressed in tensor notation and neglecting the gravity effect as follows:

Mass conservation

$$\frac{\partial}{\partial x_i} (\rho u_i) = 0 \quad (1)$$

Momentum conservation

$$\frac{\partial}{\partial x_j} (\rho u_j u_i) = -\frac{\partial P}{\partial x_i} + \frac{\partial}{\partial x_j} \left[ (\mu + \mu_t) \left( \frac{\partial u_i}{\partial x_j} + \frac{\partial u_j}{\partial x_i} \right) \right] \quad (2)$$

where,  $\rho$ ,  $\mu$ ,  $\mu_t$  and  $u_i$  are the density, molecular viscosity, eddy viscosity and time average mean flow velocity of the fluid respectively.

In the two equation  $k-\varepsilon$  model, the turbulent viscosity have a direct functional relationship with turbulent kinetic energy ( $k$ ) and its dissipation rate ( $\varepsilon$ ). These two quantities are evaluated by solving their respective conservation equations. The three  $k-\varepsilon$  models (standard, RNG and realizable) are basically differs from each other by the expression the turbulent viscosity and by the formulation of their source and sink terms.

In  $k-\varepsilon$  model, the  $k$  and  $\varepsilon$  equations are expressed as follows:

$$\frac{\partial}{\partial x_i} (\rho k u_i) = \frac{\partial}{\partial x_j} \left[ \left( \mu + \frac{\mu_t}{\sigma_k} \right) \frac{\partial k}{\partial x_j} \right] \pm S_k \quad (3)$$

$$\frac{\partial}{\partial x_i} (\rho \varepsilon u_i) = \frac{\partial}{\partial x_j} \left[ \left( \mu + \frac{\mu_t}{\sigma_\varepsilon} \right) \frac{\partial \varepsilon}{\partial x_j} \right] \pm S_\varepsilon \quad (4)$$

Within a flow, the shear rate and strain rate are higher within higher gradient zones, like boundary layer region and vortex region. But Standard  $k-\varepsilon$  model does not predict well within these region because, the model constants presents in source and sink term of  $k$  and  $\varepsilon$  are not case sensitive. On the other hand, in RNG  $k-\varepsilon$  model, the governing equations have been derived through time averaging integration from the instantaneous Navier-Stokes equations using the renormalization group (RNG) theory [24], [26]. The best feature in this model is that, the additional term is included in  $\varepsilon$  equation source term, which varies dynamically with respect to change in strain rate of the turbulence. That causes more precise predictions during the speeded or stretched flow. However an additional option in the model is incorporated to put the effects of swirl in the flow by suitably modifying the eddy viscosity using a functional form based on swirl number.

In realizable  $k-\varepsilon$  model [26], the constant used in standard  $k-\varepsilon$  model is now used as a variable, which is used to evaluate eddy viscosity and expressed as a function of mean strain rate. Moreover the source and sink term in  $\varepsilon$ -equation is different, particularly the destruction of  $\varepsilon$  is a function of shear deformation. Description of the major  $k-\varepsilon$  models are discussed in detail in ref. [29].

## B. Boundary and operating conditions

Different boundary conditions are specified at each and every boundary of the computational geometry, i.e., outlet, inlet, wall and axis of combustor (Fig. 1). A uniform axial and radial velocity component has been used at the inlet plane. The axial flow velocity ( $U_{x-in}$ ) is calculated from the Reynolds number  $1.2 \times 10^5$  by using the diameter of the inlet pipe ( $D_s$ ). The inlet tangential velocity is evaluated as;

$$U_{\theta-in} = U_{x-in} \tan \theta \quad (5)$$

The swirl number is calculated by using the following expression as;

$$SN = \frac{2}{3} \frac{(D_s^3 - D_h^3)}{(D_s^2 - D_h^2)(D_s - D_h)} \tan \theta \quad (6)$$

The boundary conditions at the inlet to initialize the governing equation for  $k$  and  $\varepsilon$  are computed from the turbulent intensity and the length scale. The length scale ( $IS$ ) and the turbulent intensity ( $TI$ ) at inlet boundary are evaluated from the expression as [30];

$$IS = 0.07 D_s \quad (7)$$

$$TI = \frac{U'}{U_{avg}} = 0.16 (\text{Re}_{Ds})^{-1/8} \quad (8)$$

No slip wall is considered for all solid walls. Standard wall function condition are used as wall boundary conditions for  $k$  and  $\varepsilon$ . Gradient along the axis of each variables are set to zero at outlet. Axis of the dump diffuser-combustor is considered as axi-symmetric boundary where all the gradients of each variable are zero.

## III. RESULTS AND DISCUSSION

### A. Grid independence test

A series of trial solutions have been performed with several quadrilateral, structured and unstructured mesh configurations, having 8100, 21300, 32200 and 41300 number elements in the domain, to ensure mesh independent results. The axial velocity variation along the radial direction at two different axial positions, i.e.  $L=0.1$  and 1.5, are compared for these mesh configurations (Fig. 2a and b). Fig. 2a shows that all the four mesh configurations predict nearly the same velocity distribution at the upstream location of the combustor ( $L=0.1$ ). However, considerable differences in the velocity distributions have been noted at the downstream location ( $L=1.5$ ) of the combustor (Fig. 2b) with the refinement of the mesh. The variation in the results progressively diminishes with the refinement of mesh and the peak change in the axial velocity falls within only 2.6% as the grid is refined from 32200 cells to 41300 cells. Finally, the mesh having 32200 elements has been selected for further computations because of computational economy.

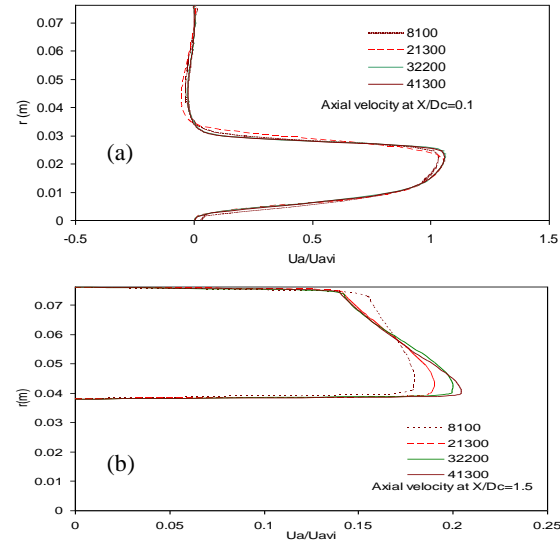


**Fig. 2 Axial velocity along the radius at various axial position (a)  $L=0.1$  (b)  $L=1.5$**

### C. Experimental validation and choice of turbulent model

The computational modeling is validated through comparison with the experimentation of Rahim et al. [16] by applying the same Reynolds number, swirl number ( $SN$ ) = 0.38, and a non-dimensional dump gap  $DG = 1$  as mentioned in the experimental work. For validation, the pressure and velocity distributions inside the pipe ahead of the dump plane, inside the sudden expansion region of the dump diffuser and within the casing-liner annulus.

### D. Flow properties in the inlet pipe before the dump plane

Fig. 3(a) to (c) depicts the comparisons of measured and the prediction of three two equation  $k-\varepsilon$  turbulent model. In these Figures, radial distributions of axial velocity, tangential velocity and static pressure, in their non-dimensional forms, at 0.05 m downstream of the inlet plane are compared against

the measurement. Fig. 3(a) shows that the peak axial velocity occurs at an off-axis radial location due to the swirling motion in the flow. The Fig. further reveals that the axial velocity is somewhat over predicted by the standard  $k-\epsilon$  model near the axis while, the other two turbulence models (RNG  $k-\epsilon$  model and realizable  $k-\epsilon$  model) under predict the axial velocity at the same region. Subsequently, beyond 40% of the pipe radius, all the three models predict nearly the same axial velocities, which remain within 4.6% of the measured values in of Rahim et al. (2007). The tangential velocity distributions predicted by the RNG  $k-\epsilon$  and realizable  $k-\epsilon$  models also show good agreement with the measured data up to 20% of the pipe radius (Fig.3b). However, some quantitative difference has been noticed in the predicted results of all the three models at higher radii. The static pressure distribution (Fig.3c) shows a low pressure region near the axis as a result of the swirling motion in the flow. All the predictive models show pressure variations similar to that of the measured one. The differences in the quantitative data reveal that the realizable  $k-\epsilon$  model predicts the pressure with the least variation from the measurement.

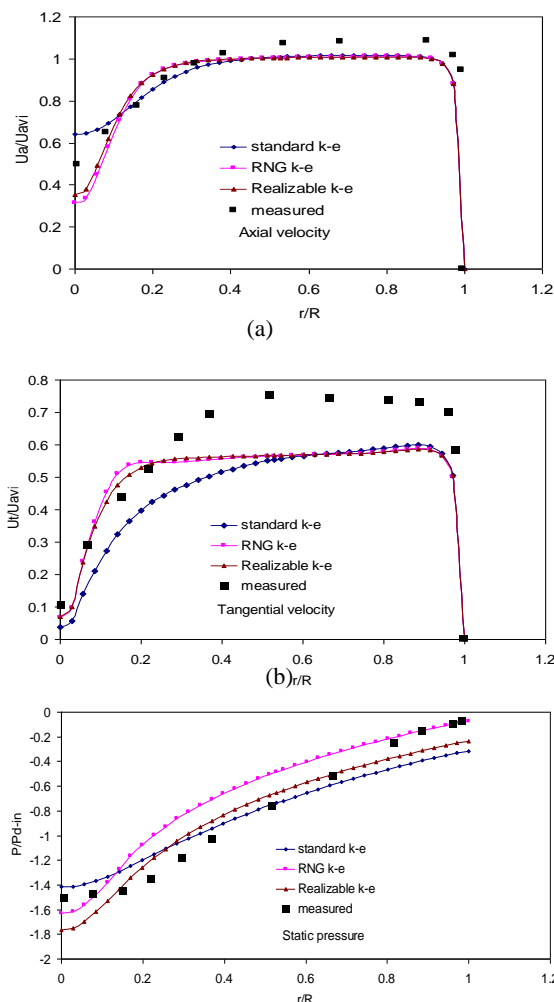


**Fig.3 Radial variation of flow parameters at 50 mm downstream from swirl inlet (a) Axial velocity (b) tangential velocity (c) static Pressure**

submitted paper should be cutting edge, result oriented, original paper and under the scope of the journal that should belong to the engineering and technology area. In the paper title, there should not be word ‘Overview/brief/ Introduction,

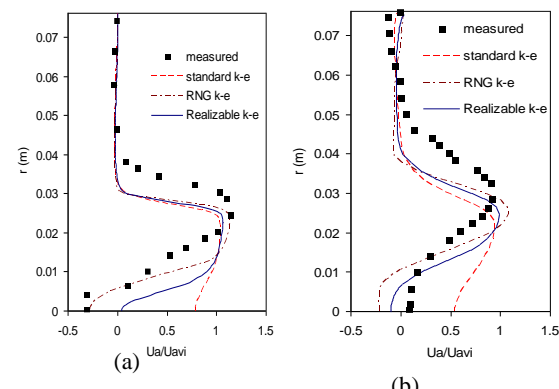
Review, Case study/ Study, Survey, Approach, Comparative, Analysis, Comparative Investigation, Investigation’.

#### E. Axial velocity distribution inside the casing and annulus

The comparison of the radial distributions of the axial velocities predicted by the numerical models and the measured data at four different axial locations (i.e.  $L=0.1$ , 0.3, 1.5 and 2.1) following the dump plane have been investigated in fig. 4a-d. Both the velocity and the distance have been plotted as non-dimensional quantities in the Fig. Fig. 4(a) shows the velocity profile at  $L=0.1$ , which lies between the dump plane and the dome head close to the dump plane. The measured data shows a flow reversal on the axis at this axial location, while a very weak back flow is also reported adjacent to the peripheral wall. Out of the three  $k-\epsilon$  models, only the RNG  $k-\epsilon$  model has predicted the on-axis back flow at this axial location, while the standard  $k-\epsilon$  model prediction shows the maximum deviation in the value. However, all the three models predict very good results near the outer wall of the casing. The peak axial velocity and its corresponding location have also been predicted fairly well by the three models.

At  $L=0.3$  (shown in Fig. 4(b)), which is near to the dome head, some change in the velocity pattern has been noticed. The measured value shows positive axial velocity on the axis, while the velocity predicted by both RNG and realizable  $k-\epsilon$  models are negative there. Standard  $k-\epsilon$  model predicts a much higher positive velocity on the axis at this plane as well. Again the peak velocity has been predicted fairly accurately by all the models.

The measured axial velocities at  $L=1.5$  and  $2.1$  (Fig. 4c and 4d) show that the flow tends to become almost uniform as it proceeds along the casing-liner annulus. Considerable differences between the measured velocities and those predicted by the RNG  $k-\epsilon$  model have been observed in these two cases inside the annulus. In fact, RNG  $k-\epsilon$  model even predicts reverse flow near the outer wall in the annulus, which is in complete disagreement with the experimental data. The axial velocity predictions from the standard and realizable  $k-\epsilon$  models, on the other hand, agree very well with the experimental measurements at these two axial locations.



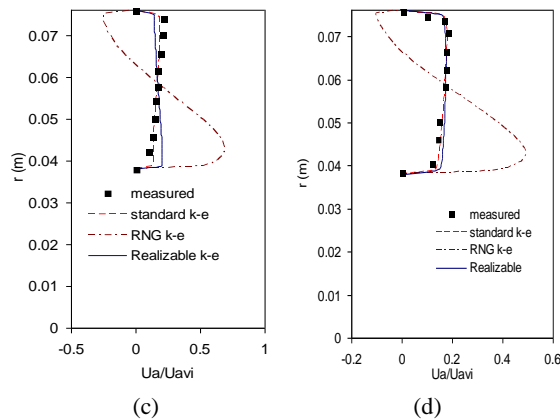


**Fig.4 Axial velocity along the radial direction at various axial position (a)  $L=0.10$  (b)  $L=0.30$  (c)  $L=1.50$  (d)  $L=2.10$**

#### F. Casing and Liner wall pressure distributions

Further to the velocities, a comparison is also made between the predicted and measured variations in the wall pressure along the casing and liner walls in Fig. 5a and 5b, respectively. The measured pressure variation shows that starting from the dump plane the pressure first decreases a little along the casing wall and then increases suddenly with a strong adverse pressure gradient. The adverse pressure gradient causes reverse flow in the recirculating vortex following the expansion. After the flow reattaches on the outer casing again the pressure changes only a little till the exit plane is reached. From fig. 5(a) it is observed that both standard  $k-\epsilon$  and the realizable  $k-\epsilon$  model predicted well of pressure variation on casing wall. However, the RNG  $k-\epsilon$  model collapses completely in its pressure prediction and shows an unrealistic pressure variation on the casing wall. Fig. 5(b) shows the non dimensional pressure over the dome and liner surface. The predicted pressure is low at the dome centre because of the swirl induced recirculation on the axis close to the dome head. The experimental data lacks sufficient resolution to describe the pressure variation on the dome surface probably due to insufficient measurement locations there. However, comparing the results it is observed that the standard  $k-\epsilon$  model and the realizable  $k-\epsilon$  model show similar trends of pressure, which are close to the measured values over most part of the liner wall.

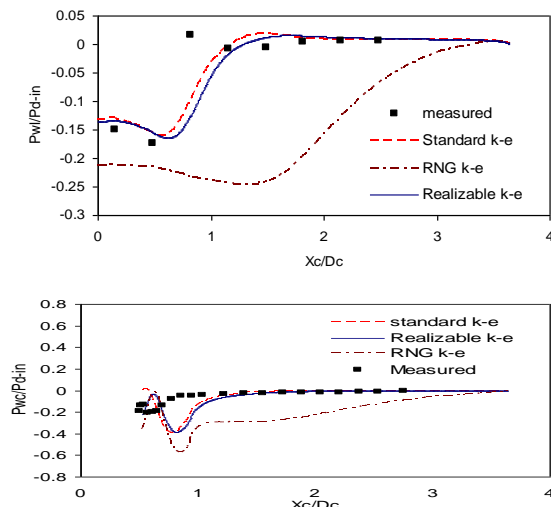


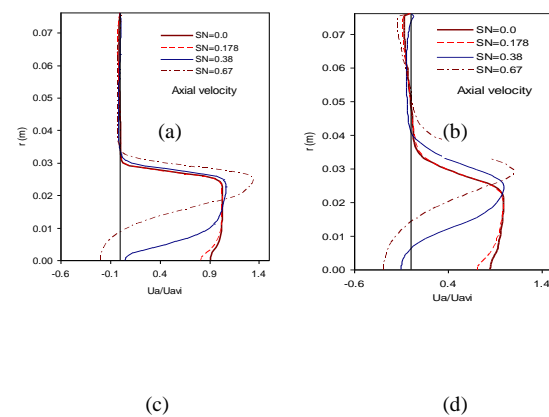
**Fig.5 Static pressure variation along the (a) Casing wall (b) Liner wall**

It is detected from the predictions of the three models that the standard  $k-\epsilon$  model performs poorly in predicting the flow in the inlet pipe after the swirler. The reverse flow observed there in the experimental measurements could not be reproduced by the standard  $k-\epsilon$  model. On the other hand, the RNG  $k-\epsilon$  model fails completely in predicting the flow velocity and pressure distribution inside the annulus region between the casing and the liner. Realizable  $k-\epsilon$  model, on the other hand, performs reasonably well over the entire domain of interest in predicting the flow velocity and pressure distribution. Therefore, the realizable  $k-\epsilon$  model has been chosen to comprehend the variation in the flow characteristics under varying operating conditions.

#### G. Effect of swirl number on flow pattern and pressure distribution

The effects of inlet swirl number on the flow patterns through the diffuser and annulus have been shown in fig. 6a-d for a dump gap of  $DG=1$ . Four different swirl numbers ( $SN$ ) of 0.0 (non-swirling), 0.178, 0.38 and 0.67 have been chosen for the study. In the non-swirling case ( $SN=0$ ), the flow coming through the inlet pipe expands in the diffuser and turns over the dome head to enter into the annulus (Fig. 6a). A stagnation point is observed at the tip of the dome in this case. A corner recirculation zone (CRZ) is formed adjacent to the dump plane as the flow separates from the wall. The flow is accelerated between the liner and the recirculating vortex. This acceleration of the main flow further stretches the CRZ to a longer size till the flow reattaches again on the casing wall.

With very weak swirl in the inlet flow ( $SN=0.178$ ), the streamline distribution does not show much difference in the flow pattern (Fig. 6b). However, on a very close observation, a tiny recirculation zone can be noticed at the tip of the dome. When the inlet swirl number increases, significant changes are observed in the flow pattern (Fig. 6c and 6d). The high swirl in the inlet flow develops a central recirculating vortex adjacent to the dome head, as the flow tends to move outwardly after reaching the plane of expansion. The size of this vortex increases with the increase in swirl number as observed from the Figures. The central vortex pull the flow in radial direction, so that the size of the corner recirculation zone is reduced. Moreover, a third vortex, which is in counter-rotating direction to the large corner recirculation vortex, is also observed at the top corner of the diffuser (Fig. 6c and 6d).



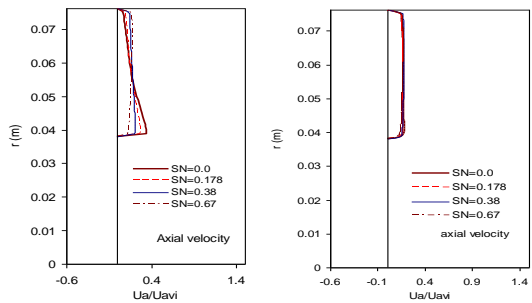


**Fig.6 Radial variation of axial velocity at different axial locations with different swirl number (a)  $L=1$  (b)  $L=0.3$  (c)  $L=1.5$  (d)  $L=2.1$**

The radial variations of axial velocity at different axial locations following the dump plane are shown in fig. 7a-d. Each of the Fig. shows the respective variations for four swirl numbers as considered in fig. 6. With zero and low swirl cases ( $SN=0$  and  $0.178$ ), no flow reversal is observed on the centerline at  $L=0.1$ . The axial velocity remains nearly constant till a certain radial location, after which it decreases rapidly across the shear layer to become negative in the corner recirculation zone. However, the magnitude of velocity in the CRZ is rather low. As the swirl number increases to  $SN=0.38$ , the centerline axial velocity considerably decreases but still remains positive. This is because the central recirculating vortex formed on the dome head is not large enough to reach the axial location. In conclusion, negative axial velocity on axial position is observed at a higher swirl number ( $SN=0.67$ ) as the central vortex extends till the dump plane. The axial velocity distribution first shows an increase from the negative value to reach the maximum and then suddenly decreases to become negative in the corner recirculation. Finally, a very small positive velocity is observed close to the outer wall of the casing due to the counter-rotating vortex existing there.

The second axial location of  $L=0.3$  also occurs before the dome head. At this axial location, centerline flow reversal is observed both for  $SN=0.38$  and  $0.67$ , as the location resides within the central recirculating vortices for the two cases. On the other hand, for the other two swirl number cases ( $SN=0$  and  $0.178$ ) the centerline axial velocities remain positive but become lower than their corresponding values at the earlier station. This is because of the radial widening of the flow. Moreover, the thickness of the shear layer, across which the velocity reduces from the maximum value to zero before turning negative for the CRZ, increases at this axial location in comparison to the previous one. The corner recirculation zone is radially shorter at this location compared to the previous location, while the reverse flow is stronger due to the increased strength of the vortex.

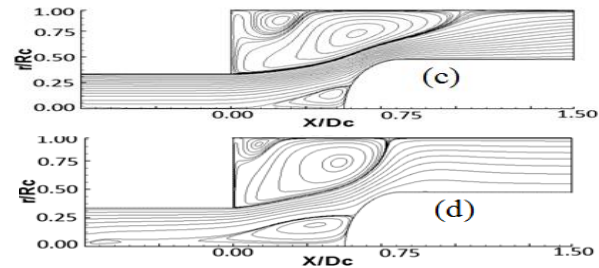
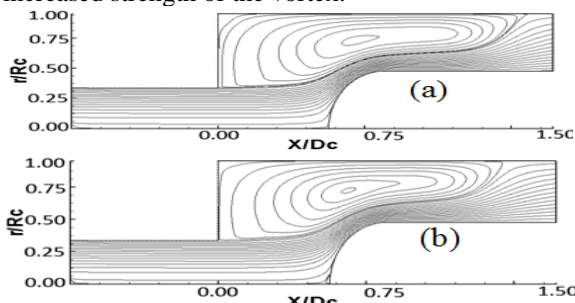


**Fig.7 Stream function at different swirl numbers (a)  $SN=0.0$  (b)  $SN=0.178$  (c)  $SN=0.38$  (d)  $SN=0.67$**

The third axial station of  $L=1.5$  is located within the casing-liner annulus at a sufficient downstream location where no flow reversal is observed in any of the four different swirl levels (Fig. 7c). However, in this case the axial velocity distribution is more uniform at higher swirl number, while at lower swirl number the axial velocity is higher near the liner wall. This is because, as the swirl number increases, the length of the CRZ decreases and therefore the flow gets more time to become radially uniform. Finally, at the last axial station considered ( $L=2.1$ ) the axial velocity pattern becomes almost similar for all the swirl numbers considered (Fig. 7d). The axial velocity at this location is uniform over the entire annular cross-section.

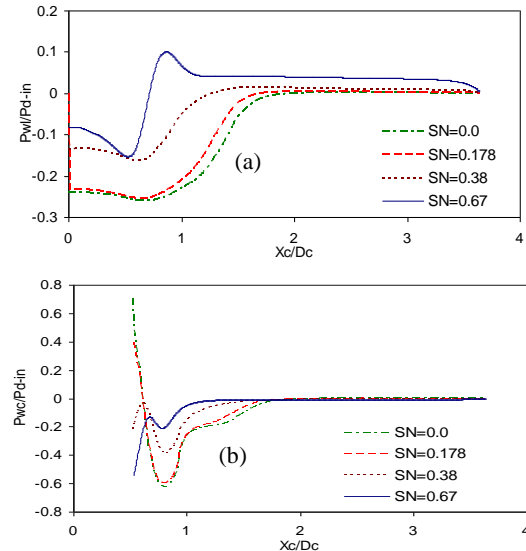


**Fig. 8 Static pressure variation with different swirl numbers along (a) Casing wall (b) Liner wall**

The pressure distributions over the walls of the outer casing and the liner, for the four different swirl cases, are plotted in fig. 8a and b, respectively. For the flow without inlet swirl and with a mild swirl ( $SN=0.178$ ), the static pressure is low near the dump inlet plane on casing wall due to CRZ formation. After which it increases rapidly to reach the maximum. The adverse pressure gradient in this region signifies the reverse flow in the corner recirculation zone. The maximum pressure point is detected at the flow reattachment position on the casing wall. Afterwards, the pressure remains nearly constant. After that a slight dropping of pressure has been observed due to viscous effect. The two pressure plots of  $SN=0$  and  $SN=0.178$  show that the recirculation length marginally decreases with the small swirl in the flow.

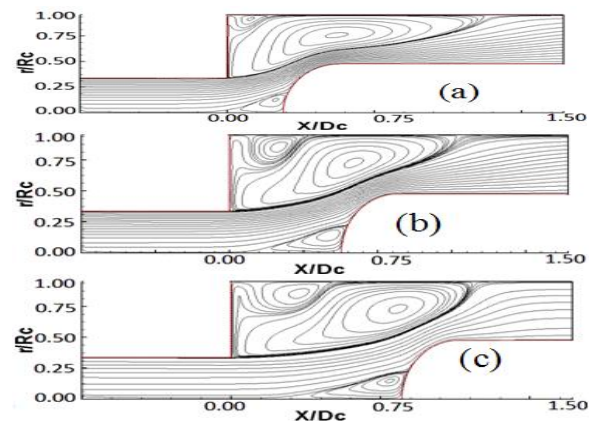
The large drop in pressure across the recirculation zone in these two cases is because of the more intense recirculating vortices driven by the accelerating main flow past them. With a relatively greater swirl intensity ( $SN=0.38$ ), the casing wall pressure variation shows a similar trend. However, the pressure near the dump inlet is higher than those in the earlier two cases, because of somewhat weaker corner recirculation zone. The flow reattachment also takes place much earlier on the casing wall as indicated by the pressure variation. In the fourth case of  $SN=0.67$ , the recirculation zone is much shorter in length and the flow reattaches on the outer wall before the liner dome takes the complete turn to make the liner wall parallel to the axis. The adverse pressure gradient is quite steep in this case and the peak pressure occurs much closer to the dump inlet. A drop in pressure is also observed after the pressure peak is reached. This drop in pressure is due to the increase in velocity that takes place after the reattachment point due to the decrease in the annular cross-sectional area.

Fig. 8(b) shows the non dimensional pressure over the dome liner at different swirl numbers. For no swirl condition, the highest pressure is noticed at the dome tip. In this condition, CTRZ is not formed at and around the dome face, hence the flow stagnation occurs just at the dome tip. With increase in flow velocity, the pressure decreases along the liner wall due to a narrow flow path available in between the recirculation vortex and the liner. Afterward as the flow path increases, flow velocity declines, hence the pressure again increases along the liner wall. The trend of liner wall pressure distribution with  $SN=0.178$  is much closer to no swirl condition. In this case, the highest pressure or stagnation point occurs at slight away from dome tip due to the formation of tiny recirculation on the dome tip due to swirl action. However, the liner wall distribution pattern of pressure along the liner is different for relatively stronger swirl. For stronger swirl having the swirl number of 0.38 and 0.67, bigger central recirculation are appeared over the dome tip. Therefore, a low pressure has been detected on the dome tip. The stagnation point occurs at the edge of the central recirculation vortex and the maximum pressure occurs there. The pressure then decreases again as the flow velocity increases after taking turn at the dome. Pressure increases when the flow velocity subsequently decreases to become flat on the liner wall.

#### H. Effect of dump gap on flow pattern and pressure distribution

Fig. 9a-c show the flow patterns following the dump plane for three different dump gaps and with  $SN=0.38$ . When the dump gap is low ( $DG=0.5$ ), the flow is turned rapidly by the liner dome. A small recirculation is formed on the central plane due to the swirl present in the inlet flow. The rapid turning accelerates the flow and stretches the corner recirculation formed on the outer casing due to higher shear. Hence a longer CRZ is appeared on the casing wall. The counter-rotating vortex is also observed at the top corner of the diffuser. After the flow reattachment on the casing wall it moves through the casing-liner annulus in the axial direction. When the dump gap is increased to  $DG=1.0$ , the central recirculation is somewhat bigger in size. The flow velocity at the dome corner is less as the flow gets more space to turn towards the periphery. As a result the volume and the strength of the CRZ decreases significantly. The corner recirculation decreases further in length when the dump gap is increased to  $DG=1.5$ . However, due to the larger space available, the

central recirculation bubble is bigger in size and the flow gets much more space to turn past the liner.



**Fig.9 Stream function with different dome gap (a) DG=0.5 (b)DG=1.0 (c) DG=1.5**

The dump gap impact on the flow reattachment point and the size of the corner recirculation can be expressed in a better way through the casing wall pressure variation along the axial direction. Fig. 10a illustrates the pressure variation on the casing wall for the three dump gap cases. It is seen that the pressure initially decreases and then increases rapidly along the wall. The initial decrease in pressure occurs over the length of the counter-rotating vortex formed on the outer wall. The adverse pressure gradients following the initial drop in pressure is owing to the flow reversal observed in the recirculating vortices. The lowest pressure is the minimum for the  $DG=0.5$  case, showing that the intensity of the recirculating eddy is the maximum for this case. For  $DG=0.5$  and 1.0, the casing wall pressure almost flattens off after accounting the corner recirculation. However, for  $DG=1.5$ , a drop in pressure is observed after the maximum pressure is reached following the adverse gradient. The drop in pressure is due to the increase in velocity owing to the reduction in flow area. The length of the corner recirculation zone can be estimated from the distance of flow reattachment from the dump plane. The result show that the recirculation vortex increases in length when the dump gap is lower.

The variations of pressure on the liner wall for the three different dump gaps are shown in fig. 10b. The plots start from different points on the abscissa depending on the location of the dome tip. The nature of the variation is similar for all the cases. Due to the formation of CTRZ over the dome tip, an adverse pressure over the dome tip is observed. Moving beyond the dome tip along the liner wall, an increase in pressure has been observed till the stagnation point is reached. After that, the liner wall pressure decreases due to increase in flow velocity because of narrowing flow path in between CRZ and liner wall. However the peak pressure at the stagnation point is almost same for all the three cases of dump gap. But, the lowest pressure obtained on liner wall is for the lowest dump gap. This is attributed to the fact that with lower dump gap the fluid is turned with a higher velocity to flow over the liner.

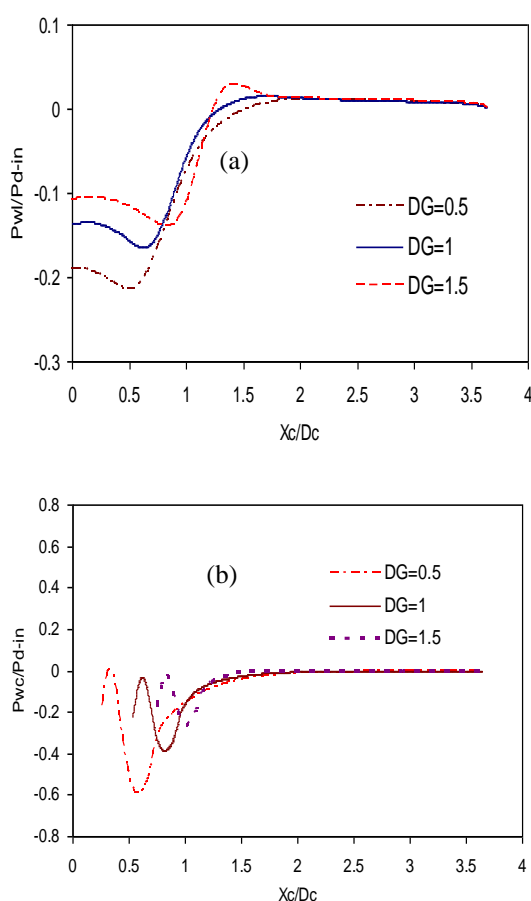


**Fig.10 Static pressure distribution with different dome gap along the (a) Casing wall (b) Liner wall**

The main purpose of a diffuser to decrease the velocity so that the static pressure can be recovered at diffuser outlet by following the Berloullian principle of energy conversion. Static pressure recovery coefficient ( $C_p$ ) is an essential parameter used for performance study of a diffuser. It is expressed as the ratio of static pressure recovery difference across the exit and inlet plane to the dynamic pressure across the inlet plane.

When a real fluid flows, there is an energy loss occur due to the formation of boundary layer. Within a flow through dump diffuser, a significant energy loss occurs by viscous dissipation due to formation of CRZ. Moreover presence of swirl also causes energy loss by forming an additional central recirculation zone. Therefore by neglecting these loses or by assuming the fluid is ideal, an ideal static pressure recovery is;

$$C_{p_{ideal}} = \left[ 1 - \frac{1}{(A_2/A_1)^2} \right], \text{ where, } A_1 \text{ and } A_2 \text{ are the cross sectional area of outlet and inlet respectively.}$$

An overall effectiveness of static pressure recovery, in percentage, expressed as,

$$\eta = \frac{C_{p_{measured}}}{C_{p_{ideal}}} \times 100$$

In Table 2. the static pressure recovery coefficient and the overall effectiveness for different inlet swirl numbers are listed, when the dump gap is kept as  $DG=1.0$ . The effectiveness in pressure recovery depends on the energy

dissipation in the eddy, which in turn depends on the eddy size and strength.

**Table-II: Static Pressure Recovery Coefficient and Overall Effectiveness at different swirl number for dump gap position (DG = 1.0)**

SN	$C_p$	$\eta (\%)$
0.0	0.226	23.29
0.178	0.346	35.61
0.38	0.580	59.69
0.67	0.523	53.82

With mild swirl, the CRZ is larger in size, causing a sizeable energy dissipation within it. This reduces the overall effectiveness of pressure recovery. At a high inlet swirl level, the corner recirculation zone becomes smaller in size. But a central recirculating bubble is formed at the dome head resulting additional loss. Therefore there should be some optimum swirl level in order to achieve the best pressure recovery. However the flow at a swirl number of 0.38 gives the best pressure recovery with a particular dump gap (DG = 1.0).

The dump gap impact on the recovery of static pressure is given in Table 3 when the air is admitted with inlet swirl number of 0.38. It has been comprehended that the dump gap offers a positive impact on pressure recovery and the overall effectiveness. When the dump gap is low, the flow is deflected towards the casing wall at a higher velocity due to flow restriction through dome. This induces a high shear on the recirculating vortex following the dump plane increasing its intensity. As a result, the energy dissipation in the vortex is large and the effectiveness in static pressure recovery is relatively small. When the dump gap increases, the flow gets more space after crossing the dump plane and gradually gets deflected outward. As a result, the intensity of the corner eddy decreases and the energy loss also decreases. As a result, along with inlet swirl, the effectiveness of pressure recovery increases with increase in dump gap.

**Table-III Effect of DG on static pressure recovery coefficient and overall effectiveness at different swirl levels**

DG	$C_p$	$\eta (\%)$
0.5	0.456	46.92
1.0	0.580	59.69
1.5	0.651	66.97

#### IV. CONCLUSIONS

A cold flow simulation in a dump diffuser-combustor has been studied numerically. Particularly flow field and pressure distribution within the inlet pipe, dump plane and annulus region has been analyzed.

Performance predictions of three major two equation  $k-\varepsilon$  models are compared against the experimental results. It has been found that overall performance of the realizable  $k-\varepsilon$  model is comparatively better than the others models in the given flow situation. The flow pattern and pressure distribution under different inlet swirl level and dump gap have been analyzed using the realizable  $k-\varepsilon$  model. The recirculation zones formed in the domain under different flow and geometrical conditions and their effects on the velocity and pressure distributions have been studied.

From the study it has been observed that, the flow employed with swirling effect forms a central recirculating vortex on the dome head tip, hence corner recirculation size is reduced. The flow within the annulus also become more uniform with the presence of swirl. It has been shown that the static pressure recovery across the diffuser depends on the dimensions and strength of the recirculation vortices (CTRZ, CRZ) formed in the flow. The static pressure can be recovered most effectively with an optimum level of inlet swirl ( $SN=0.38$ ) in the flow for a particular dump gap ( $DG=1.0$ ).

The dump gap significantly affects the dimension and strength of the recirculation zones. Increment of dump gap improvises the static pressure recovery with an inlet moderate swirl of ( $SN=0.38$ ).

It can be concluded from the results that in a gas turbine combustor, the outlet guide vanes should be properly designed to provide the optimum swirl level in the flow entering the combustor. The dump gap should be decided based on the static pressure recovered, space required for the injector and optimum size and weight of the engine.

## V. NOMENCLATURE

Cross-sectional area [m <sup>2</sup> ]	$U_x$	axial velocity [ms <sup>-1</sup> ]
Static Pressure recovery coefficient	$U_\theta$	tangential velocity [ms <sup>-1</sup> ]
Diameter of casing [m]	$u$	velocity vector
Non-dimensional dump gap (Ld/Dl)	$X$	Axial distance from dump inlet plan [m]
Static pressure [Nm <sup>-2</sup> ]	$\theta$	Swirl angle [deg]
Dynamic pressure at inlet [Nm <sup>-2</sup> ]	$\eta$	Overall efficiency of pressure recovery
Radius of inlet pipe [m]	<b>Subscript s</b>	
Radius of the casing [m]	i, j	Subscript for axial or radial velocity notation
Reynolds number	in	inlet
Radial distance [m]	1	Swirl inlet
swirl number	2	Exit of combustor

## REFERENCES

1. A. H. Lefebvre and D. R. Ballal, Gas turbine combustion: alternative fuels and emissions: CRC press, 2010.
2. A. D. Walker, J. F. Carrotte, J. J. McGuirk, "Enhanced external aerodynamic performance of a generic combustor using an integrated OGV/prediffuser design technique, Journal of engineering for gas turbines and power " vol. 129, pp. 80-87, 2007.
3. D.L. Rhode, D. G. Lilley, and D. K. McLaughlin, "On the prediction of swirling flowfields found in axisymmetric combustor geometries," vol. 104, pp. 378-384, 1982.
4. A. S. Green and J. H. Whitelaw, "Isothermal models of gas-turbine combustors" Journal of Fluid Mechanics, vol. 126, pp. 399-412, 1983.
5. J. J. McGuirk, J. M.L.M Palma, "The flow inside a model gas turbine combustor: Calculations," vol. 115, pp. 594-602, 1993.
6. S. Mondal, A. Datta, and A. Sarkar, "Influence of side wall expansion angle and swirl generator on flow pattern in a model combustor calculated with  $k-\varepsilon$  model" International journal of thermal sciences, vol. 43, pp. 901-914, 2004.
7. A. F. Bicen, W. P.Jones, "Velocity characteristics of isothermal and combusting flows in a model combustor" Combustion science and technology, vol. 49, pp. 1-15, 1986.
8. M. Heitor, J.H. Whitelaw, "Velocity, temperature, and species characteristics of the flow in a gas-turbine combustor" Combustion and Flame ,vol. 64, pp. 1-32, 1986.
9. A. Datta and S. K. Som, "Combustion and emission characteristics in a gas turbine combustor at different pressure and swirl conditions" Applied Thermal Engineering , vol. 19, pp. 949-967, 1999.
10. S. Patil, S. Abraham, D. Tafti, S. Ekkad, Y. Kim, P. Dutta, H.-K. Moon, and T. Srinivasan, "Experimental and numerical investigation of convective heat transfer in a gas turbine can combustor" ASME Turbo Expo 2009: Power for Land, Sea, and Air, pp. 1363-137.
11. C.R. Fishenden and S. J. Stevens, "Performance of annular combustor-dump diffusers" Journal of Aircraft, vol. 14, pp. 60-67, 1977.
12. K.C. Karki, V. L. Oechsle, and H.C. Mongia, "A computational procedure for diffuser-combustor flow interaction analysis," in ASME 1990 International Gas Turbine and Aeroengine Congress and Exposition, 1990.
13. R. Hestermann, S. Kim, A. B. Khaled, and S. Wittig, "Flow field and performance characteristics of combustor diffusers: a basic study," in ASME 1994 International Gas Turbine and Aeroengine Congress and Exposition, 1994.
14. A. D. Walker, J. F. Carrotte, J. J. McGuirk, "The influence of dump gap on external combustor aerodynamics at high fuel injector flow rates" Journal of engineering for gas turbines and power, vol. 131, p. 031506, 2009.
15. A. Rahim, S. Veeravalli, and S. Singh, "Effect of inlet swirl and dump-gap on the wall pressure distribution of a model can-combustor," 2002.
16. A. Rahim, S.N. Singh, S. V. Veeravalli, Part A: Journal of Power, and Energy, "Liner dome shape effect on the annulus flow characteristics with and without swirl for a can-combustor model" Proceedings of the Institution of Mechanical Engineers, Part A: Journal of Power and Energy, vol. 221, pp. 359-368, 2007.
17. V. S. Kumar, A. Sameen, H. Kim, T. Setoguchi, S. Mastuo, and S. Raghunathan, "Influence Of Dump Gap On The Performance Characteristics Of Dump-Diffusers."
18. S. H. Chuang, H. C. Lin, F. M. Tai, and H. M. Sung, "Hot flow analysis of swirling sudden-expansion dump combustor" International journal for numerical methods in fluids, vol. 14, pp. 217-239, 1992.
19. P. Moin and S. V. Apte, "Large-eddy simulation of realistic gas turbine combustors" AIAA journal , vol. 44, pp. 698-708, 2006.
20. S. James, J. Zhu, and M. S. Anand, "Large-eddy simulations as a design tool for gas turbine combustion systems" AIAA journal, vol. 44, pp. 674-686, 2006.
21. M. Sanjosé, J. Senoner, F. Jaegle, B. Cuenot, S. Moreau, and T. Poinsot, "Fuel injection model for Euler–Euler and Euler–Lagrange large-eddy simulations of an evaporating spray inside an aeronautical combustor" International Journal of Multiphase Flow, vol. 37, pp. 514-529, 2011.
22. G. Heidarnejad and S. Delfani, "Direct numerical simulation of the wake flow behind a cylinder using random vortex method in medium to high reynolds numbers" International Journal of Engineering, vol. 13, pp. 33-50, 2000.
23. P. J. Foster, J. M. Macinnes, F. Schubnell, "Isothermal modelling of a combustion system with swirl: A computational study" Combustion science and technology, vol. 155, pp. 51-74, 2000.
24. A. Escue and J. Cui, "Comparison of turbulence models in simulating swirling pipe flows" Applied Mathematical Modelling, vol. 34, pp. 2840-2849, 2010.
25. R. Shafaghat and Y. Vazifeshenas, "Numerical simulation of cavitation in mixed flow pump" International Journal of Engineering, vol. 28, pp. 956-963, 2015.

26. J. Zhu and T. H. Shih, "Computation of confined coflow jets with three turbulence models" International journal for numerical methods in fluids, vol. 19, pp. 939-956, 1994.
27. I. Karagoz, F. Kaya, CFD investigation of the flow and heat transfer characteristics in a tangential inlet cyclone" International Communications in Heat and Mass Transfer, vol. 34, pp. 1119-1126, 2007.
28. L. Yajun, Z. Hongtao, M. Yong, and C. Biyong, "Application of Turbulent Models on Simulation of Intense Swirling Flow Combustor," in 2011 Asia-Pacific Power and Energy Engineering Conference, 2011.
29. Ansys Fluent, "Theory Guide 13.0," 2010.Ansys Fluent, "User Guide (Release 13.0).

### AUTHORS PROFILE



**Mr. Ajay Kumar Sahu** is a PhD. Scholar working on solid fuel combustion. He received his master degree from University college of Engineering, Burla, Odisha.



**Dr. Prakash Ghose** received his PhD. degree from Jadavpur University Kolkata. He has done his master degree from University college of Engineering , Burla, Odisha. Now he is working as Asst. Professor in KIIT Deemed to be University, Bhubaneswar. He published more than 16 articles in different journals and conferences. His research interest is Heat Transfer and combustion.